High Power Laser Science and Engineering, (2024), Vol. 12, e55, 9 pages.
doi:10.1017/hpl.2024.43

HIGH POWER LASER SCIENCE AND ENGINEERING

RESEARCH ARTICLE

High beam quality 10 kW light source based on thin-film beam combination

Dongdong Li[1,2,3,4], Xinshang Niu[1,2,3,4], Xiaochuan Ji[1,2,3,4], Hongfei Jiao[1,2,3,4], Jinlong Zhang[1,2,3,4], Yujie Xing[1,2,3,4], Jian Zhang[1,2,3,4], Xiong Dun[1,2,3,4], Xinbin Cheng[1,2,3,4], and Zhanshan Wang[1,2,3,4]

[1] *Institute of Precision Optical Engineering, School of Physics Science and Engineering, Tongji University, Shanghai, China*

[2] *Key Laboratory of Advanced Micro-structured Materials, Ministry of Education, Tongji University, Shanghai, China*

[3] *Shanghai Frontiers Science Center of Digital Optics, Shanghai, China*

[4] *Shanghai Professional Technical Service Platform for Full-Spectrum and High-Performance Optical Thin Film Devices and Applications, Shanghai, China*

(Received 12 April 2024; revised 31 May 2024; accepted 17 June 2024)

Abstract

Thin-film beam combining technology is an effective approach to improve output power while maintaining beam quality. However, the lack of comprehensive research into the key factors affecting the beam quality in systems makes it challenging to achieve a practical combined beam source with high brightness. This paper clearly established that the temperature rise of dichroic mirrors (DMs) and sub-beam overlapping precision are the main factors affecting the beam quality of the system, with quantified effects. Based on this understanding, a combined light source of four channels of 3 kW fiber lasers was achieved, and an output power of 11.4 kW with a beam quality of $M^2_x = 1.601$ and $M^2_y = 1.558$, using three high-steepness low-absorption DMs and the active control technique. To the best of our knowledge, this is the best beam quality for a 10 kW light source. This study offers a solution for practical high-power laser sources in the tens of kilowatts range.

Keywords: 10 kW light source; beam quality; overlapping precision; temperature rise; thin-film beam combining technology

1. Introduction

The demand for laser sources to destroy small targets, such as drones, requires laser sources that have both high beam quality and a power of tens of kilowatts[1–5]. Fiber lasers are the ideal light source for this purpose due to their compact structure, high efficiency, good beam quality and stable and reliable operation[2–4,6]. However, nonlinear effects, thermal effects, mode instability and other factors set a theoretical limit to the output power of a single laser[7–13], which does not meet the requirements of the high-power laser range.

Thin-film beam combining (TFBC) technology is an effective approach to increasing laser output power while maintaining beam quality and is therefore a hot topic in the field of high-power laser technology research[14–17]. It primarily utilizes dichroic mirrors (DMs) to selectively transmit lasers of different wavelengths efficiently within a given bandwidth, while allowing efficient reflection of lasers of a different bandwidth, thereby achieving the combination of multiple sub-beams[14,18–20]. This technology has relatively low requirements for parameters such as sub-beam wavelength, line width and polarization state. DMs can reduce the line-width requirements of sub-beams to a few nanometers, requiring fewer components, and having a simpler and more reliable optical layout, compact structure, easy integration, and suitability for more flexible combat scenarios.

TFBC technology has shown significant advantages in low-power combining. Regelskis *et al.*[21] initially proposed combining a three-pulse fiber laser based on DMs, while preserving the beam quality of a single laser. However, with the increase of combining power, this technology is facing challenges. Chen *et al.*[22] found that although an output power of 10.12 kW was achieved when combining two continuous fiber lasers with a power of 5 kW, the beam quality deteriorated significantly and reached $M^2_x = 11.4$ and

Correspondence to: Jinlong Zhang, Institute of Precision Optical Engineering, School of Physics Science and Engineering, Tongji University, Shanghai 200092, China. Email: jinlong@tongji.edu.cn

$M^2_y = 10.4$. Further experiments revealed that one of the main reasons for this deterioration was the thermal effects of the DMs. This understanding propelled further research. Subsequently, Zheng *et al.*[23] realized the combination of three 4 kW single-mode lasers with an output power of 11.34 kW by optimizing the thickness of DMs to reduce their thermal absorption. The beam quality was measured to be $M^2_x = 2.941$ and $M^2_y = 3.183$. To completely avoid the effects of temperature rise in the DMs, Ludewigt *et al.*[5] utilized three low-power 2 kW lasers for beam combining, achieving an output power of 5.9 kW with a beam quality of $M^2 = 1.9$. The entire device is integrated into a compact space, demonstrating the miniaturization advantages of DM beam combination. Xi *et al.*[24] verified the feasibility of achieving high beam quality with TFBC technology using a three-channel broadband fiber laser, with an output power of 13.52 kW and a beam quality of 1.61. Sun *et al.*[25] achieved an output of 9.6 kW with a beam quality of 1.7 using a three-channel fiber laser in the laboratory.

The above research demonstrates significant progress in TFBC technology based on DMs that achieve power output of up to 10 kW. However, it is difficult to achieve high power output and excellent beam quality at the same time. Most of the research work is still in the laboratory validation stage and has not reached the practical application level. Researchers have recognized that the thermal effect of DMs is one of the main factors affecting beam quality. They have proposed measures to reduce the temperature rise of DMs to improve the quality of the system. However, there is a lack of fundamental research and understanding of the quantitative relationship between temperature rise and beam quality. Furthermore, other key factors affecting the beam quality of combining systems have not been discussed. It is therefore necessary to systematically analyze and study the key factors that contribute to the deterioration of beam quality in systems to overcome the key challenge of achieving high power output while maintaining high beam quality in combined light sources.

In order to solve the above problems, the influence of the temperature rise in the DMs and the precision of sub-beam combination on the beam quality of TFBC systems was analyzed in detail in this paper, and their fundamental relationship with the beam quality was clarified. By using low-absorption DMs and a precise angle control technique, the temperature rise of the DMs was effectively reduced, the accuracy of the sub-beam combination was improved and high beam quality of the system was realized. Finally, we used three DMs to combine four continuous fiber lasers with central wavelengths of 1060, 1070, 1080 and 1090 nm, respectively. We achieved an output power of 11.47 kW, beam quality of $M^2_x = 1.601$, $M^2_y = 1.558$ and beam combining efficiency of 95.3% for the combined light source. This research achievement provides solid theoretical support for the realization of high beam quality light sources.

2. Main factors influencing the beam quality of the combining system

The TFBC system mainly uses DMs to combine multiple sub-beams, inevitably considering three main factors that affect the beam quality of the system. The first is the sub-beam quality, which is determined by the design and industrial technology of the individual laser sources, and represents the best beam quality that the combining system can achieve. The second is the temperature rise of DMs resulting in a thermal lens that deteriorates the beam quality and the shape of the sub-beams that pass through it. The third is the precision of sub-beam overlap, which determines the quality of the combined beam. The factors influencing the beam quality of individual sub-beam lasers are not discussed in this paper.

2.1. Theoretical analysis of the temperature rise of a dichroic mirror with influence on the beam quality

The increase in temperature of DMs leads to distortion of mirror and refractive index change, which changes optical path difference, resulting in beam focusing, divergence or shift of the beam[26]. When the temperature varies radially, the change in refractive index and temperature is represented as in Equation (1). The change in optical path difference is then described by Equation (2)[27].

$$\Delta n(r)_T = \Delta T(r) \cdot \frac{\mathrm{d}n}{\mathrm{d}T}, \tag{1}$$

$$\Delta\delta_{\mathrm{OPD}} = n_0 L + \Delta\delta_{\mathrm{thermal}}(r) + \Delta\delta_{\mathrm{stress}}(r) + \Delta\delta_{\mathrm{expansion}}(r), \tag{2}$$

where $\Delta n(r)_T$ is the material refractive index with the change in temperature, $\Delta T(r)$ is the change in temperature of the DM, $\mathrm{d}n/\mathrm{d}T$ is the temperature-induced change in the refractive index, n_0 is the material refractive index at a constant temperature, L is the length of the optical path, $\Delta\delta_{\mathrm{thermal}}(r)$ is the change in optical path length due to change in the refractive index, as shown in Equation (3), $\Delta\delta_{\mathrm{stress}}(r)$ is the change in optical path length due to the photoelastic effect for isotropic materials stress, as shown in Equation (4), and $\Delta\delta_{\mathrm{expansion}}(r)$ is the change in optical path length due to a change in crystal length due to thermal expansion, as shown in Equation (5).

$$\Delta\delta_{\mathrm{thermal}}(r) = L\Delta n(r)_T, \tag{3}$$

$$\Delta\delta_{\mathrm{stress}}(r) \approx -\frac{n_0^3}{2}\rho\alpha L\Delta T(r), \tag{4}$$

$$\Delta\delta_{\mathrm{expansion}}(r) \approx 2\alpha n_0 w\Delta T(r), \tag{5}$$

where ρ is the photoelastic coefficient, α is the thermal expansion coefficient and w is the spot radius of the beam after collimation.

https://doi.org/10.1017/hpl.2024.43 Published online by Cambridge University Press

From the above analysis, it can be concluded that the temperature rise of DMs causes three types of thermal effects that change the optical path difference of the beam. This changes the beam passing through the DMs affected by the temperature and consequently reduces the beam quality of the individual laser.

2.2. Theoretical analysis of the influence of the sub-beam overlapping accuracy on the beam quality

The sub-beam overlap accuracy is determined by the angular or positional deviation. The angular deviation reflects the non-parallelism of each sub-beam optical axis, while positional deviation reflects the central positions of each sub-beam spot. If the angular deviation increases, the positional deviation also increases with increasing distance from the laser effect. However, in applications where the laser acts at a long distance, the angular deviation is the primary factor and positional error has a minor impact on the angular error, so that only correction of the angular error is required[28]. The wavelength beam combining technology studied in this paper is aimed at applications at considerable distances and focuses on the quality of far-field beams, so that angular deviation is the primary factor.

If two laser beams propagate over a large distance L, the precision of the overlap of the two sub-beam spots in the far field can be calculated as shown in Equation (6):

$$\eta = 1 - \frac{2}{\pi}\arcsin\left(\frac{\pi L\theta\cdot\tan\delta}{2\lambda}\right) - \frac{L}{\pi}\cdot\tan\delta\cdot\sqrt{\frac{\pi^2\theta^2}{\lambda^2} - \frac{\pi^4L^2\theta^4\cdot\tan^2\delta}{4\lambda^4}}, \quad (6)$$

where η is the overlapping accuracy of two lasers, δ is the angular deviation of the two lasers, θ is the divergence angle of the laser far-field beam, $\theta = 2\lambda/(\pi w)$, λ is the average wavelength of the overlapping beam and w is the radius of the sub-laser.

The above indicates that overlap accuracy decreases with increasing angular deviation of the sub-beams. To ensure good overlap accuracy of the two sub-beams in the far field, it is required that $\eta \geq 86.5\%$. At this point, the angular deviation is $\delta \leq \theta$, where θ represents the maximum angular deviation of the two sub-beams.

Further, we introduce how to calculate the deflection angles of the two sub-beams, that is, focusing the combination beam onto the face of the angle detector. By using the detector to detect and calculate the centroid positions of the sub-beam spots, the maximum angular deviation of the two sub-beams' overlap is calculated as shown in Equation (7):

$$\sigma = \sqrt{\sigma_x^2 + \sigma_y^2}, \quad (7)$$

where σ_x is the angular deviation in the x-direction, $\sigma_x = \delta\cdot\Delta_x/f$, σ_y is the angular deviation in the y-direction, $\sigma_y = \delta\cdot\Delta_y/f$, δ is the resolution of the detector, Δ_x and Δ_y are the offset of the beam in the x- and y-directions on the detection surface and f is the focal length of an optical lens.

If $\sigma \leq \theta$, then it is judged that the sub-beam lasers overlap completely. The higher the accuracy of σ, the higher the precision of sub-beam overlap.

3. Experimental verification

Based on the above analysis, experimental setups were respectively constructed to investigate the influence of DM temperature rise and sub-beam combination angle accuracy on the beam quality of the combining system.

3.1. Relationship between DM temperature rise and laser beam quality

We have set up an experiment to study the relationship between DM temperature rise and beam quality, the overall scheme of which is shown in Figure 1. The laser wavelength is 1070 nm with a power range of 1800–9000 W, with an interval of 900 W. A thermal imager is used to monitor

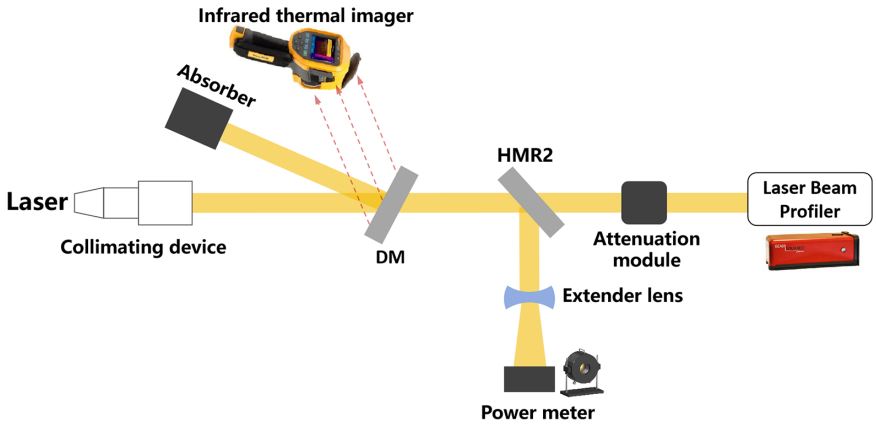

Figure 1. Schematic of experimental setup to test relationship between the DM temperature rise and the laser beam quality.

https://doi.org/10.1017/hpl.2024.43 Published online by Cambridge University Press

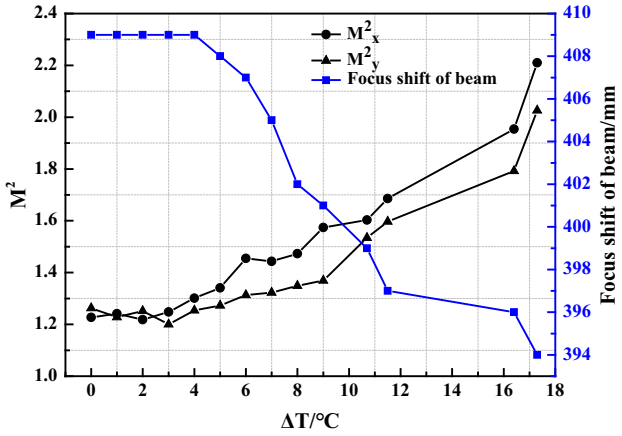

Figure 2. The influence of temperature rise of the DM on the beam quality and beam focus position.

and record the temperature changes of the DM in real time, as described in the physical properties paper of the DM referenced by Li *et al.*[26]. The laser irradiates the DM after collimation, with part of the laser passing through, and a small portion of the reflected laser is received by the absorber. The transmission laser passing through high reflectivity mirror 2 (HRM2) primarily reflects most of its power through the extender lens into the power meter, while a smaller portion of the power further undergoes attenuation through the attenuation module to meet the energy requirements for entry into the laser beam profiler. The laser beam profiler detects and calculates the changes in beam quality, beam spot morphology and beam focal point position in real time. The experimental results are shown in Figures 2 and 3.

As shown in Figure 2, the temperature rise of the DM is within 5°C, and the beam quality of the laser and the focus position remain basically unchanged. When the temperature rise reaches 5°C, the spot morphology and beam quality begin to change slightly, and the focal point position also begins to shift. Beyond 5°C, the beam quality deteriorates significantly, and the displacement of the focal point position gradually increases. As shown in Figure 3, the spot morphology in the far field remains unchanged within 4°C and maintains a good Gaussian distribution. At 5°C, the spot morphology begins to deteriorate. The central energy begins to diverge, leading to an uneven distribution, and the focus position also begins to change. After 5°C, the beam spot morphology deteriorates significantly. At 10°C and 17°C, it can be observed that the central energy of the spot is essentially dispersed, corresponding to a significant displacement of the focus position.

The research results indicate that the thermal effect of the DM is the main reason for the degradation of single-laser beam quality. The higher the temperature, the worse the beam quality, the more severe the deterioration of spot morphology and the greater the deviation of the beam focus position.

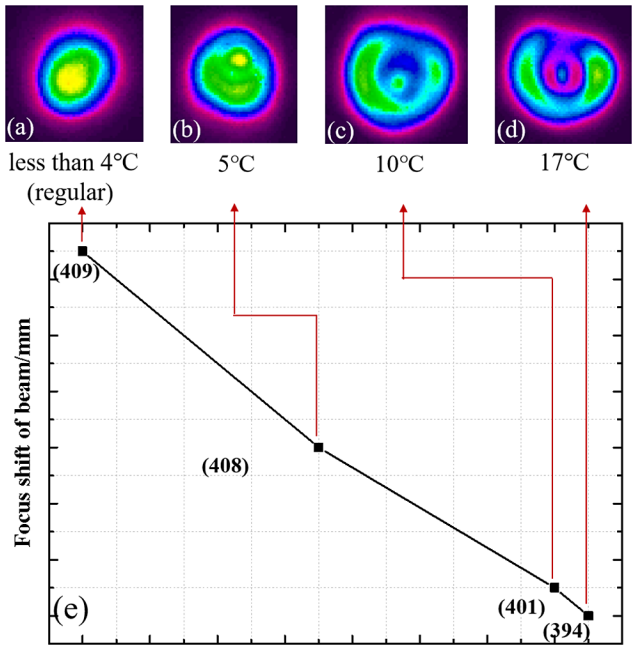

Figure 3. The influence of the DM with different temperatures on the far-field spot and focus offset of beam.

3.2. Relationship between the sub-beam angular deviation and beam quality

An experimental setup for investigating the influence of angular deviation on the beam quality of two sub-beam lasers in the far field is illustrated in Figure 4. The transmitted beam of collimated sub-beam laser 2 passing through the DM overlaps with the reflected beam of collimated sub-beam laser 1, which passes through high reflectivity mirror 1 (HRM1) and the DM. The overlapping beam passes through HRM2, with most of the energy being directed into the power meter after the extender lens, while a small portion of the reflected laser enters the laser beam profiler after passing through the attenuating module. In this process, the angle deviation of the two sub-beams in the far-field beam can be changed by adjusting HRM1. Laser 1 and Laser 2 are sub-beams with wavelengths of 1060 and 1070 nm, respectively, and a minimum power setting of 300 W. The specific parameters are shown in Table 1. The DM has a low absorption and no temperature increase when irradiated by the two sub-beams at low power levels. According to theoretical calculations, the maximum angle deviation for the overlap of the two sub-beams is 27.1 μrad. The experimental results are shown in Figures 5 and 6.

As shown in Figure 5, the change in beam quality M^2 increases as the angle of deviation of the sub-beams increases. The relationship between angular variation and beam quality follows a parabolic trend, with quality deteriorating as deviation increases. Angular deviation plays a decisive role in determining the beam quality of the combined beam.

https://doi.org/10.1017/hpl.2024.43 Published online by Cambridge University Press

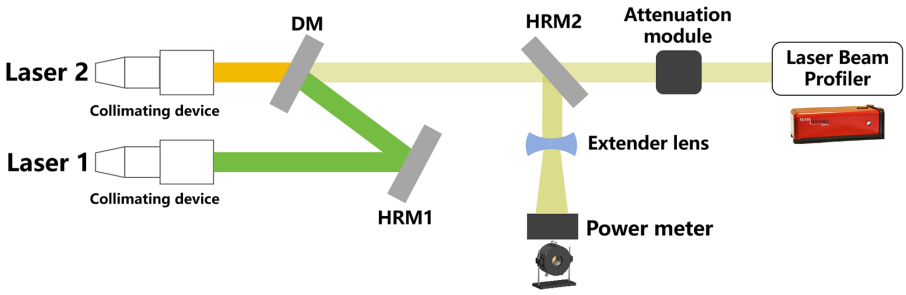

Figure 4. Angular deviation test diagram of the two sub-beam lasers overlapping in a far-field spot.

Table 1. Key parameters of the sub-beam fiber laser (measured results).

Name	Sub-beam laser 1	Sub-beam laser 2	Sub-beam laser 3	Sub-beam laser 4
λ	1060.17 nm	1069.84 nm	1080.24 nm	1089.84 nm
Δλ	0.8169 nm@20 dB	0.9019 nm@20 dB	0.7986 nm@20 dB	0.7803 nm@20 dB
Output power	3005 W	3010 W	3008 W	3013 W
Beam quality	$M^2_x = 1.246$	$M^2_x = 1.234$	$M^2_x = 1.254$	$M^2_x = 1.228$
	$M^2_y = 1.238$	$M^2_y = 1.209$	$M^2_y = 1.248$	$M^2_y = 1.279$

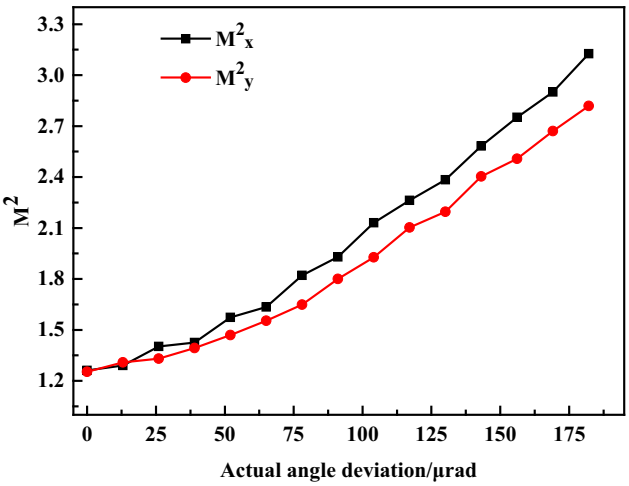

Figure 5. The relationship between angular deviation and beam quality.

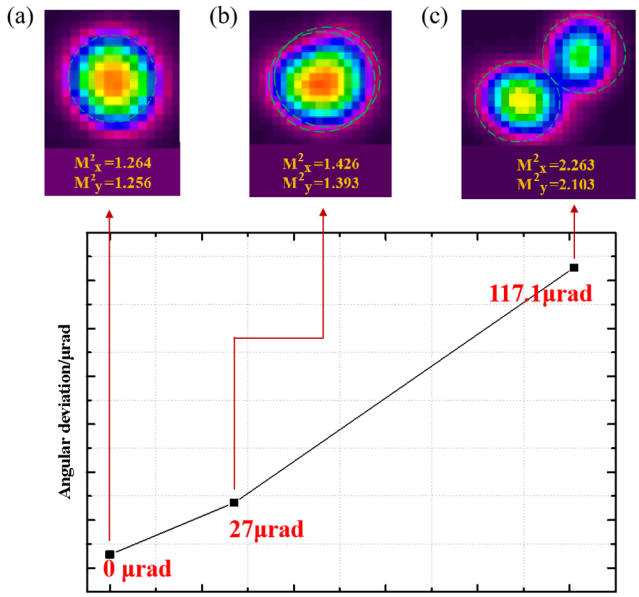

Figure 6. Angular overlap of the two sub-beam lasers at the focus position. (a) When the two sub-beams overlap almost completely, the quality of the combined beam is consistent with that of a single beam, and the corresponding angular deviation is close to 0 μrad. (b) When the two sub-beams are in a state of maximum overlap, the beam quality of the combined beam is slightly higher than that of a single beam, and the corresponding angular deviation is 27 μrad. (c) When the two sub-beams are completely separated, the beam quality of the combined beam deteriorates severely, and the corresponding angular deviation is 117.1 μrad.

Figure 6 shows data on the angular overlap precision of sub-beam spots and beam quality under three different states. Figure 6(a) shows that the sub-beam spots basically overlap when the deviation angle of the sub-beam approaches zero, and that the quality of the combination beam is consistent with that of a single-path beam. The combination beam spot has excellent morphology that resembles a Gaussian distribution. Figure 6(b) shows that the maximum deviation angle under the overlap of the sub-beams is 27 μrad, which is essentially consistent with theoretical analysis. However, the actual combination beam quality has started to change, with an increment of 0.18, and the spot morphology also begins to change slightly. The results indicate that there is an angular deviation that inevitably leads to degradation in combined beam quality. It is necessary to improve the angular resolution to meet the precision requirements for close angular overlap. Figure 6(c) shows that the angular deviation when the sub-beams are completely separated is 117.1 μrad and the increase in beam quality is approximately 1. This shows that the angular overlap accuracy of the sub-beams has a significant impact on the beam quality and determines the beam quality of the combined beam.

Theoretical analysis and experimental results indicate that light sources with high power and beam quality can be

https://doi.org/10.1017/hpl.2024.43 Published online by Cambridge University Press

realized if the temperature rise of the DMs and the angular deviation of the combined sub-beams can be controlled. By keeping the temperature rise of the DMs within 5°C and the angular deviation better than 27 μrad, the beam quality of the wavelength combining system approaches that of a single laser beam.

4. High beam quality 10 kW thin-film beam combining system

4.1. Low-absorption dichroic mirror and active control technology

The design of DMs is mainly based on the Fabry–Pérot thin-film optical cavity theory, and OptiLayer is used for detailed design of the DMs. The substrate material is sapphire with a thickness of 10 mm and a working angle of 15°. The physical structure diagram obtained from the design is shown in Figure 7(a). The measured spectrum of the DM is shown in Figure 7(b). The measured transmittance of the three DMs is greater than 97%. The reflectance of 1060 DM3, 1070 DM2 and 1080 DM1 is more than 99.9% over a wide range from 1065, 1075 and 1085 to 1100 nm, respectively.

We have developed an active real-time control technology that includes high-precision devices to monitor the sub-beam angle and high-resolution fast-steering mirrors to control the sub-beam alignment, as shown in Figure 8. The monitoring device monitors the position data of sub-beam laser spots in real time, uses algorithms to calculate the position, compares it with theoretical positions and forwards the error data back to the fast-steering mirror device. Using algorithms, it dynamically controls the orientation of the reflecting mirror, ensuring real-time control of the beam's orientation to guarantee combination accuracy. When monitoring the angular deviation, a device with a monitoring accuracy of 8.86 μrad is primarily used to acquire the angular information of the sub-beams in real time, as shown in Figure 8(a). It adjusts the position of the reflectors in real time through the fast-steering mirror to ensure the position of the sub-beams in the image plane. The monitoring device and adjustment were discussed in detail by Li *et al.*[26]. The fast-steering mirror device dynamically adjusts the orientation of sub-beams in real time based on feedback data, with a resolution of more

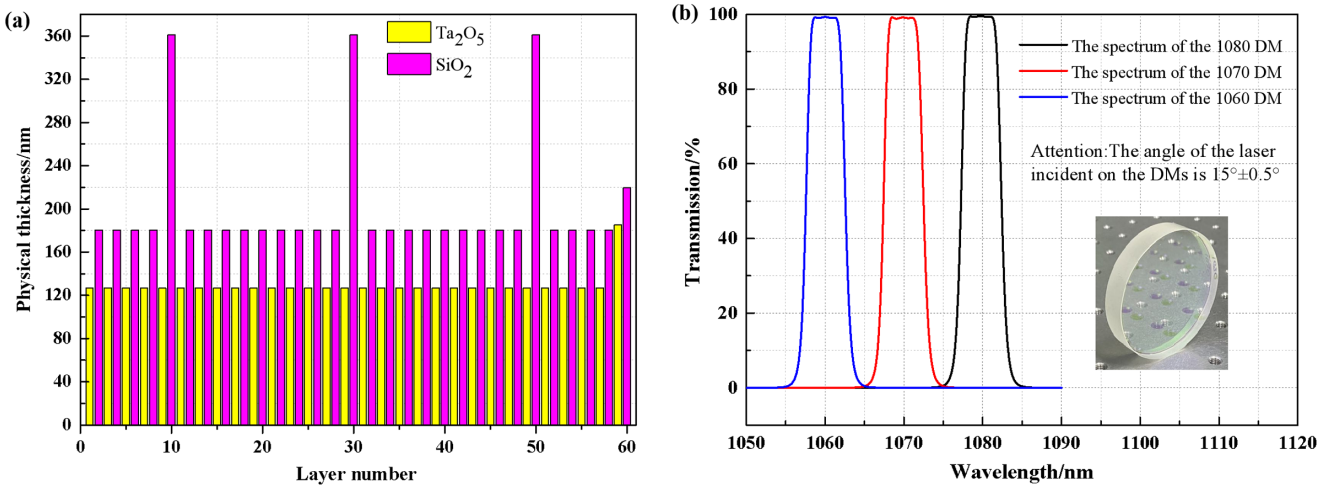

Figure 7. Physical structure design and the measured spectrum of the DMs. (a) The physical structure of the DM designed using OptiLayer. (b) Measured spectra of the three types of DMs.

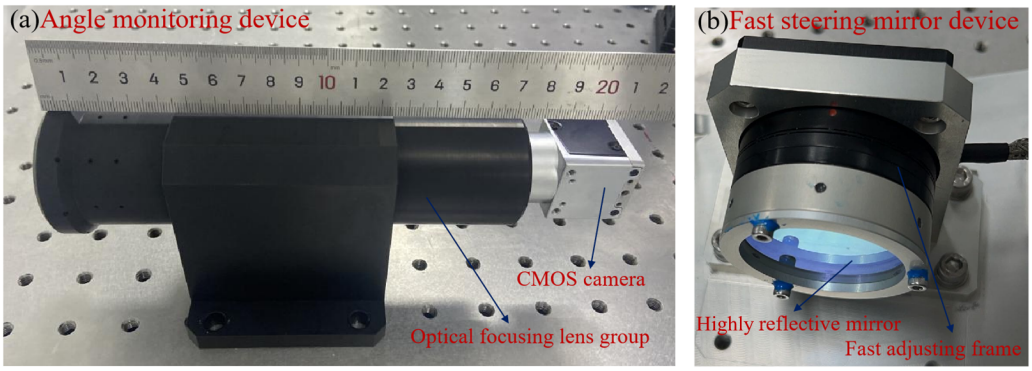

Figure 8. Active control technology hardware. (a) Angle monitoring device. (b) Fast-steering mirror device.

https://doi.org/10.1017/hpl.2024.43 Published online by Cambridge University Press

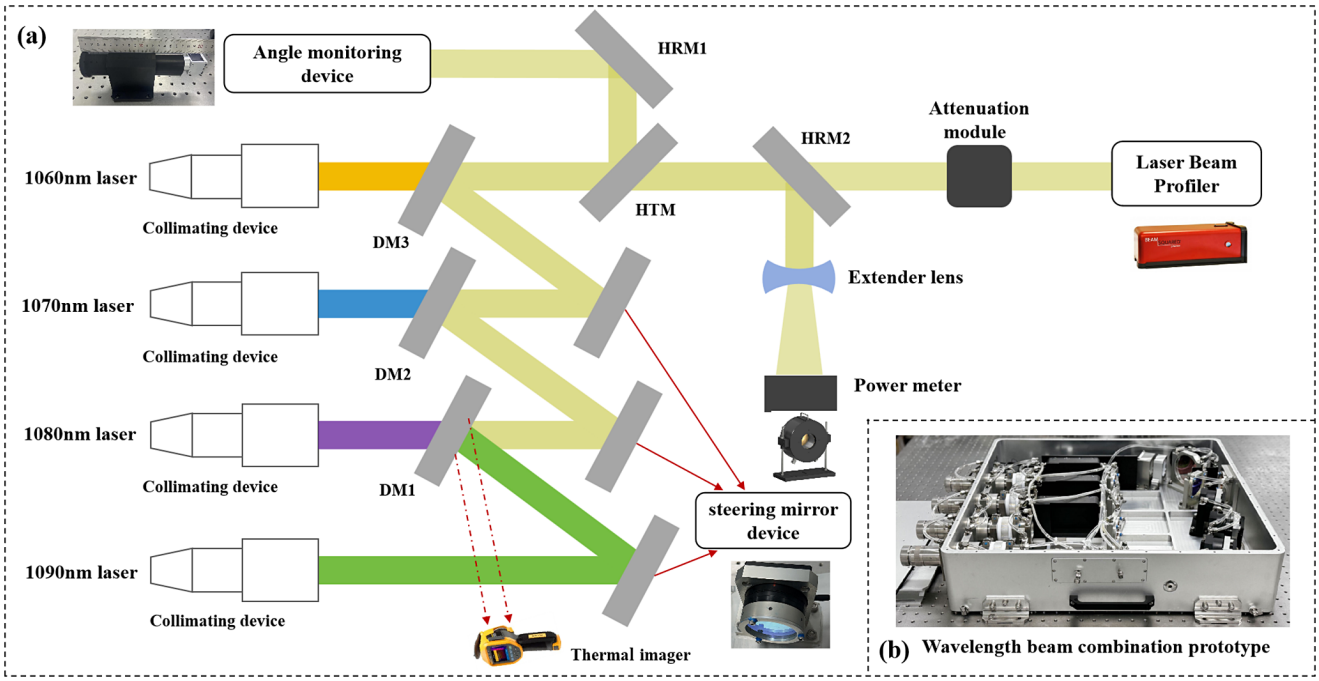

Figure 9. Overall structure diagram. (a) Performance testing for the prototype of the wavelength combined source. (b) Physical diagram of the beam combination system prototype.

than 0.5 μrad and a resonant frequency exceeding 1000 Hz for payloads of up to 150 g, as shown in Figure 8(b).

4.2. Practical combined laser source

Based on the above theoretical and experimental studies, three DMs are used in this work to achieve the co-aperture wavelength combination of four fiber lasers and obtain a prototype light source with high power and beam quality. Among them, the DM has high transmission, high reflection, high damage threshold and good thermal stability in continuous operation, and meets the requirement of extremely low absorption, as shown in Figure 7. The sub-beam fiber laser is a continuous fiber laser with a narrow linewidth and relatively good beam quality, whose technology is mature and stable. The key parameters are listed in Table 1.

Each sub-beam laser is designed with a collimating mirror to collimate the output laser and achieve approximately parallel light emission for transmission and combination. The combination beam passes through a high-transmission mirror (HTM), reflecting a small portion of its energy to HRM1 and enters the angle detection device. The HTM allows most of the combined beam energy to pass through, and then it proceeds to HRM2, which reflects most of the energy. After passing through the beam extender lens, it enters the power meter, while a small portion of the laser continues to pass through an attenuation module before entering the laser beam profiler. The integration was completed in a small beam combining device, as shown in Figure 9(b). Finally, the performance of the combined beam light source was measured experimentally, as shown in the schematic diagram in Figure 9(a). The reflectance of HRM2 is 99.92%, and its absorption is very small, so there is no temperature rise in HRM2 after irradiation.

4.3. Experimental results of the light source with thin-film beam combination

According to the constructed measurement setup shown in Figure 9(a), the key parameters of the combined beam source were measured, as shown in Figure 10. Figure 10(a) shows that the measured combined beam power reaches 11.47 kW and the calculated efficiency of the beam combination is 95.3%. Figure 10(b) shows that under full power irradiation, the DM shows no temperature rise, with the surface temperature of the mirror at 24.1°C. Figure 10(c) demonstrates that under full power irradiation, the four combined sub-beams essentially overlap completely and have a favorable beam profile with good beam quality, achieving $M^2_x = 1.601$ and $M^2_y = 1.558$. However, the combined beam quality still exhibits an increase of approximately 0.3 compared to that of a single fiber laser, which is primarily due to slight variations in beam quality due to angular deviations in each sub-beam, which is consistent with theoretical analysis. We can further enhance beam angle precision and ensure beam quality by adjusting the resolution of the angle deviation monitor. After subjecting the light source to wheel transport vibration and wide temperature tests, the beam quality detection results remain within 1.6. The transportation vibration parameters include a vibration frequency of 200 r/min and an amplitude

https://doi.org/10.1017/hpl.2024.43 Published online by Cambridge University Press

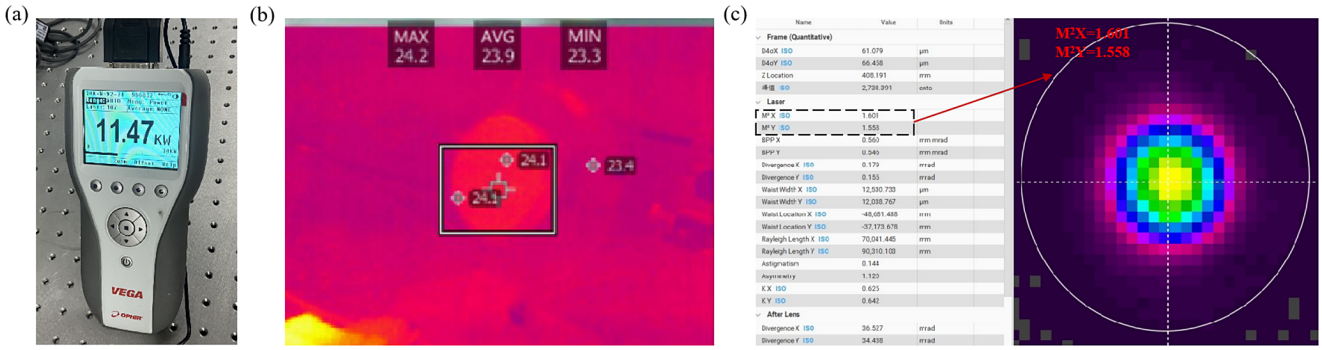

Figure 10. Performance parameters of the combined beam light source. (a) Power of the combined beam light source. (b) Temperature rise of the DM under full power irradiation. (c) Beam quality of the combined beam light source at full power.

of 25.4 mm. The wide temperature parameters range from –20°C to 70°C.

In summary, we have developed an integrated and practical light source with high brightness. Moreover, the DM experiences no temperature rise under a single 3 kW laser irradiation, indicating that it can withstand stronger laser irradiation. With the same number of combined paths that increase the power of single lasers, along with high-precision monitoring devices, it is possible to achieve laser light sources with tens of kilowatts power and high beam quality.

5. Conclusion

In this work, we systematically analyzed the most important factors affecting the beam quality of the combined beam source. It became clear that the temperature rise of DMs and the precision of sub-beam combination angle are the main reasons for the deterioration of the beam quality of the system. The maximum power density that DMs (without temperature rise) can withstand determines the maximum power and beam quality of the single laser, while the precision of the sub-beam combination angle determines the beam quality of the beam combining system. Finally, three DMs are used to achieve beam combining of four fiber lasers. The result is a compact beam combining light source with a high beam quality of $M^2_x = 1.601$, $M^2_y = 1.558$, an output power of 11.47 kW and an efficiency of 95.3%. The combined beam quality degradation data examined in this paper provide a reliable basis for the realization of high beam quality laser sources in the tens of kilowatts range.

Acknowledgements

This work was supported by the National Natural Science Foundation of China (Nos. 62061136008, 62275196, 62192772, 62305251, 61925504, 61975153, 6201101335, 62020106009, 62192770 and 61621001), Science and Technology Commission of Shanghai Municipality (Nos. 17JC1400800, 20JC1414600 and 21JC1406100), Special Development Funds for Major Projects of Shanghai Zhangjiang National Independent Innovation Demonstration Zone (No. ZJ2021-ZD-008), Shanghai Municipal Science and Technology Major Project (No. 2021SHZDZX0100), Fundamental Research Funds for the Central Universities, and National Key R&D Program of China (No. 2022YFA1603403).

References

1. K. Ludewigt, T. Riesbeck, B. Schünemann, A. Graf, and A. Tünnermann, Proc. SPIE **8547**, 854704 (2012).
2. K. Ludewigt, T. Riesbeck, A. Graf, and M. Jung, Proc. SPIE **8898**, 88980N (2013).
3. K. Ludewigt, T. Riesbeck, T. Baumgrtel, J. Schmitz, A. Graf, and M. Jung, Proc. SPIE **9251**, 92510N (2014).
4. M. Jung, T. Riesbeck, J. Schmitz, T. Baumgärtel, K. Ludewigt, and A. Graf, Proc. SPIE **10254**, 1025416 (2017).
5. K. Ludewigt, A. Liem, U. Stuhr, and M. Jung, Proc. SPIE **11162**, 1116207 (2019).
6. A. Tünnermann, T. Schreiber, F. Röser, A. Liem, S. Höfer, H. Zellmer, S. Nolte, and J. Limpert, J. Phys. B **38**, 681 (2005).
7. Y. Aoki, K. Tajima, and I. Mito, J. Lightwave Technol. **6**, 710 (1988).
8. J. W. Dawson, M. J. Messerly, R. J. Beach, M. Y. Shverdin, E. A. Stappaerts, A. K. Sridharan, P. H. Pax, J. E. Heebner, C. W. Siders, and C. P. J. Barty, Opt. Express **16**, 13240 (2008)
9. M. N. Zervas and C. A. Codemard, IEEE J. Sel. Top. Quantum Electron. **20**, 219 (2014).
10. J. Man, P. Ma, L. Huang, J. Xu, P. Zhou, and X. Gu, High Power Laser Sci. Eng. **5**, e30 (2017).
11. S. Fu, W. Shi, Y. Feng, L. Zhang, Z. Yang, S. Xu, X. Zhu, R. A. Norwood, and N. Peyghambarian, J. Opt. Soc. Am. B **34**, A49 (2017).
12. C. Shi, Q. Sheng, S. Fu, S. Sun, J. Zhang, W. Shi, and J. Yao, Opt. Express **28**, 2948 (2020).
13. P. Ma, H. Xiao, W. Liu, H. Zhang, X. Wang, J. Leng, and P. Zhou, High Power Laser Sci. Eng. **9**, e45 (2021).
14. T. Y. Fan, IEEE J. Sel. Top. Quantum Electron. **11**, 567 (2005).
15. O. Schmidt, C. Wirth, D. Nodop, J. Limpert, T. Schreiber, T. Peschel, R. Eberhardt, and A. Tünnermann, Opt. Express **17**, 22974 (2009).
16. E. Bochove, IEEE J. Quantum Electron. **38**, 432 (2002).
17. S. J. Augst, A. K. Goyal, R. L. Aggarwal, T. Y. Fan, and A. Sanchez, Opt. Lett. **28**, 331 (2003).

https://doi.org/10.1017/hpl.2024.43 Published online by Cambridge University Press

18. T. H. Loftus, A. Liu, P. R. Hoffman, A. M. Thomas, M. Norsen, R. Royse, and E. Honea, Opt. Lett. **32**, 349 (2007).
19. T. H. Loftus, A. M. Thomas, P. R. Hoffman, M. Norsen, R. Royse, A. Liu, and E. C. Honea, IEEE J. Sel. Top. Quantum Electron. **13**, 487 (2007).
20. C. Wirth, O. Schmidt, I. Tsybin, T. Schreiber, T. Peschel, F. Brückner, T. Clausnitzer, J. Limpert, R. Eberhardt, A. Tünnermann, M. Gowin, E. ten Have, K. Ludewigt, and M. Jung, Opt. Express **17**, 1178 (2009).
21. K. Regelskis, K. Hou, G. Raciukaitis, and A. Galvanauskas, in *Conference on Lasers and Electro-Optics/Quantum Electronics and Laser Science Conference and Photonic Applications Systems Technologies* (Optica Publishing Group, 2008), paper CMA4.
22. F. Chen, J. Ma, C. Wei, R. Zhu, W. Zhou, Q. Yuan, S. Pan, J. Zhang, Y. Wen, and J. Dou, Opt. Express **25**, 32783 (2017).
23. Y. Zheng, M. He, X. Liu, Z. Ma, J. Chen, M. Yu, S. Li, Y. Cao, and X. Wang, Laser Optoelectron. Progress **60**, 227 (2023).
24. X. Xi, B. Yang, P. Wang, H. Zhang, X. Wang, K. Han, Z. Wang, X. Xu, and J. Chen, Acta Phys. Sin. **72**, 184203 (2023).
25. R. Sun, K. Zhang, L. Zhang, X. Zhang, T. Wu, and H. Zhao, High Power Laser Particle Beams **35**, 121004 (2023).
26. D. Li, X. Niu, J. Xia, H. Jiao, X. Dun, J. Zhang, X. Cheng, and Z. Wang, Opt. Commun. **552**, 130034 (2024).
27. J. D. Mansell, J. Hennawi, E. K. Gustafson, M. M. Fejer, R. L. Byer, D. Clubley, S. Yoshida, and D. H. Reitze, Appl. Opt. **40**, 366 (2001).
28. D. Li, J. Xia, X. Niu, H. Jiao, J. Zhang, X. Dun, D. Xue, Z. Zhang, X. Cheng, and Z. Wang, Opt. Express **32**, 1512 (2024).

https://doi.org/10.1017/hpl.2024.43 Published online by Cambridge University Press